ACS OMEGA

http://pubs.acs.org/journal/acsodf

Article

[^{99m}Tc]Tc-DTPA-Bis(cholineethylamine) as an Oncologic Tracer for the Detection of Choline Transporter (ChT) and Choline Kinase (ChK) Expression in Cancer

Ambika Parmar Jaswal, Puja Panwar Hazari,* Surbhi Prakash, Pallavi Sethi, Aruna Kaushik, Bal G. Roy, Swati Kathait, Baljinder Singh, and Anil Kumar Mishra*

Cite This: *ACS Omega* 2022, 7, 12509−12523

Read Online

ACCESS | Metrics & More | Article Recommendations | Supporting Information

ABSTRACT: Objective: The elevated choline transporters (ChT), choline kinase (ChK), choline uptake, and phosphorylation in certain tumor cells have influenced the development of radiolabeled choline derivatives as diagnostic probes for imaging cell membrane proliferation. We, therefore, aimed to develop a choline-based moiety for imaging choline kinase-overexpressed tumors by single-photon emission tomography (SPECT). A novel choline-based diagnostic probe was synthesized and evaluated preclinically in various ChT- and ChK-overexpressed tumor models for SPECT imaging applications. Methods: The synthesis of diethylenetriaminepentaacetic acid-bis-choline ethylamine [DTPA-bis(ChoEA)] featured the conjugation of dimethylaminoethanol to a bifunctional chelator DTPA anhydride. [^{99m}Tc]Tc-DTPA-bis(ChoEA) was prepared, and its in vivo characteristics were evaluated in BALB/c mice and tumor-xenografted PC3, A549, and HCT116 athymic mouse models. The in vitro parameters, including cell binding and cytotoxicity, were assessed in PC3, A549, and HCT116 cell lines. To evaluate the specificity of the radioprobe, competitive binding studies were performed. Small-animal SPECT/CT diagnostic imaging was performed for in vivo evaluation. The mouse biodistribution data was further investigated to estimate the radiation dose in humans. Results: In silico studies suggested high binding with enhanced specificity. A standard radiolabeling procedure using stannous chloride as a reducing agent showed a labeling yield of 99.5 ± 0.5%. The in silico studies suggested high binding with enhanced specificity. [^{99m}Tc]Tc-DTPA-bis(ChoEA) showed high in vitro stability and specificity. The pharmacokinetic studies of [^{99m}Tc]Tc-DTPA-bis(ChoEA) in mice showed an increased tumor-to-background ratio after few minutes of intravenous administration. The first-in-human trial was also conducted. The effective dose was estimated to be 0.00467 mSv/MBq (4.67 mSv/GBq), resulting in a radiation dose of up to 1.73 mSv for the 370 MBq injection of [^{99m}Tc]Tc-DTPA-bis(ChoEA). Conclusions: The synthesized radioprobe [^{99m}Tc]Tc-DTPA-bis(ChoEA) accumulates specifically in choline kinase-overexpressed tumors with a high signal-to-noise ratio. The preclinical and first-in-man data suggested that [^{99m}Tc]Tc-DTPA-bis(ChoEA) could potentially be used as a diagnostic SPECT tracer in the monitoring and staging of cancer.

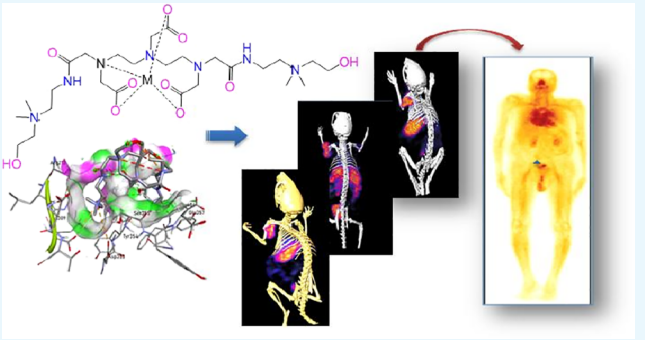

INTRODUCTION

The present clinical management strategies in cancer diagnosis demand a highly specific approach capable of validating diagnosis with pathology, exactly isolating tumor volume, grading tumors, tumor staging, treatment response, and reoccurrence along with minimal exposure to the patient. Anomalous cell growth is a distinctive attribute associated with oncological conditions involving abrupt cell proliferation and thus requires increased energy to sustain increased cell division and growth. All these processes which cause reprograming of cellular metabolism are cancer characteristics.[1] In clinical scenarios, molecular imaging techniques such as positron emission tomography (PET), single-photon emission computed tomography (SPECT), and so forth are considered as the most potent adjuncts in histopathology for the grading and staging of tumors.[2] Methionine, choline, glucose, acetate, tyrosine, and dopamine are few of the biomolecules which are used as PET radioprobes clinically for tumor diagnosis and staging.[3] Early diagnosis of tumor prevents malignant transformations, thereby facilitating better clinical prognosis.[4] Furthermore, these biomolecules when used as radiotracers in PET imaging result in differential uptake in some human

Received: September 2, 2021
Accepted: March 8, 2022
Published: April 8, 2022

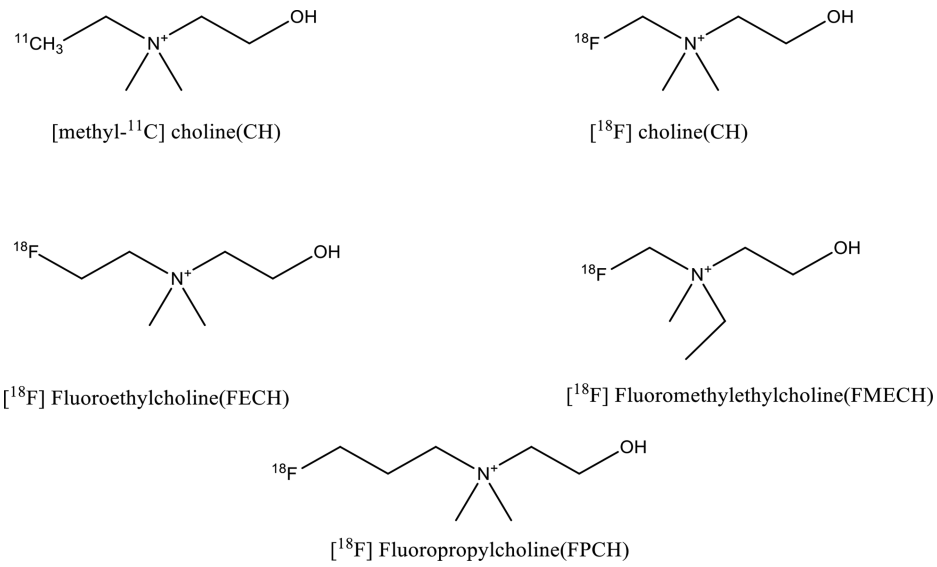

Figure 1. Chemical structures of reported radiolabeled choline analogues.

cancers, which is considered to be a clinically useful tool for diagnostic and staging.[5] Molecular imaging of cancer with ^{18}F and ^{11}C choline analogues (Figure 1) with equivocal results has been already demonstrated by various groups.[6]

Anomalous choline metabolism has been reported to be associated with oncogenesis and cancer progression.[7] Various intermediate enzymes, metabolites, and transporters involved in choline metabolism are considered as biomarkers in the progression of various cancers such as breast,[8] ovarian,[9,10] colorectal,[11] prostate,[12] lung,[13] autoimmune disease,[14] endometrial,[15] pancreatic[16] cancer, and so forth. Altered membrane choline phospholipid metabolism has been associated with the transformation of healthy cells to malignant cells.[17] It has been reported that in PET imaging, the specific PET signal is shown by the transport and phosphorylation of the radiotracer to ^{11}C phosphocholine.[18] Choline kinase, which is profoundly found to increase in many tumors and catalyzes the conversion of choline to phosphocholine, leads to the trapping of phosphocholine in cells. This whole metabolic process of choline kinase activity forms the basis for investigation of choline analogues as radioprobes for tumor imaging. The increase in intracellular choline mediated through choline transporters serves as a prerequisite for cancer cell proliferation.[18−20] The specific transport mechanism and phosphorylation by choline kinase are the two mechanisms associated with choline integration into cells where choline is trapped inside the cells as phosphocholine.[20] The radiolabeled choline uptake at the target organ is mainly due to transport, phosphorylation and oxidation.[21] ^{11}C- and ^{18}F-labeled choline analogues have already been proven to be superior to [^{18}F]F-FDG.

The structural properties and stearic interferences imparted in the choline backbone by ^{18}F introduction have been explored thoroughly both under in vitro and in vivo conditions; these studies demonstrated that the two methyl groups are important for maintenance of molecule affinity for choline kinase specificity and for choline transport system, whereas the third methyl group can be modified or replaced by an alkyl chain where radionuclide is linked.[22−25] [^{18}F]F-FCH and [^{18}F]F-FECH are the two most utilized choline analogues in clinical practice.[26] The structures of various reported choline analogues are shown in Figure 1.

[^{18}F]F-FDG is widely and successfully accepted in clinical scenarios for the diagnosis of various tumors.[1,3,4] However, decreased specificity and sensitivity due to its glucose metabolism targeting feature[27] and high bladder accumulation with renal clearance which interferes with the visualization of the tumors of the pelvic region[28] are the limitations associated with its use.

Motivated by the clinical use of choline analogues as PET radioprobes for tumor imaging, we have reported a choline analogue DTPA-bis-(cholineethylamine) [DTPA-bis-(ChoEA)] for SPECT-based applications, which could be utilized as a PET radioprobe when labeled with ^{68}Ga. The ^{99m}Tc complexation of the synthesized choline analogue DTPA-bis(ChoEA) has been validated by rhenium complexation. Rhenium is a third-row transition-metal congener of technetium, which exhibits similar complexation chemistry to technetium and is often used as a surrogate for ^{99m}Tc radiopharmaceutical characterization.[29] DTPA-bis(ChoEA) has been synthesized and evaluated in PC3, A549, and HCT116 human cancer cell lines and athymic tumor models in accordance with the animal usage guidelines.[30] Comparative studies of [^{99m}Tc]Tc-DTPA-bis(ChoEA) and [^{18}F]F-FECH were also carried out in healthy BALB/c mice.

Our aim of developing a SPECT probe based on choline was to provide a cost-effective, easily available, effortless radiopharmacy, and kit-based formulation for clinical applications. The synthesis of a SPECT radioprobe involves the covalent conjugation of quaternized dimethylaminoethanol to DTPA. Among all the known SPECT radioisotopes, ^{99m}Tc has gained an advantage for the development of new radioprobes because of its in-house generator-based availability, an acceptable half-life of 6 h, an optimal 140 KeV gamma energy, and cost-effective pharmacy.[31]

The dosimetry aspects of [^{99m}Tc]Tc-DTPA-bis(ChoEA) have been evaluated for the translation of the synthesized radioprobe for the clinical visualization of tumors with altered choline metabolism. For the clinical translation of a radioprobe, it is important to weigh the risk versus benefit from any medical radiation exposure. Accordingly, it becomes man-

https://doi.org/10.1021/acsomega.1c04256
ACS Omega 2022, 7, 12509−12523

Scheme 1. (A) Synthetic Strategy Followed for the Synthesis of DTPA-Bis-(cholineethylamine); (B) Plausible [^{99m}Tc]Tc-DTPA-Bis(ChoEA) Complex

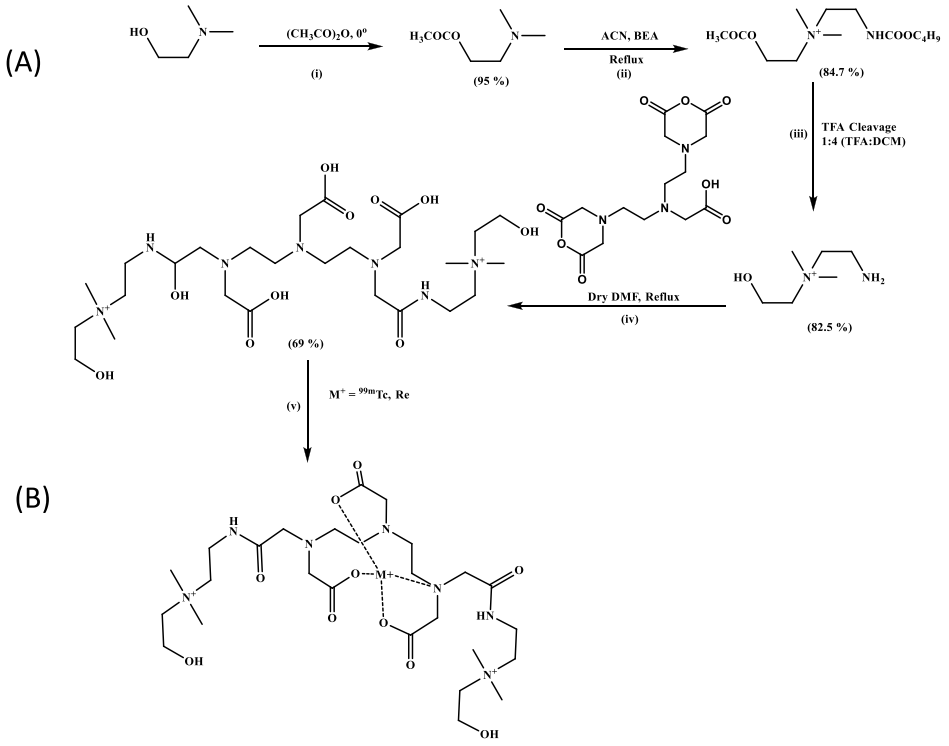

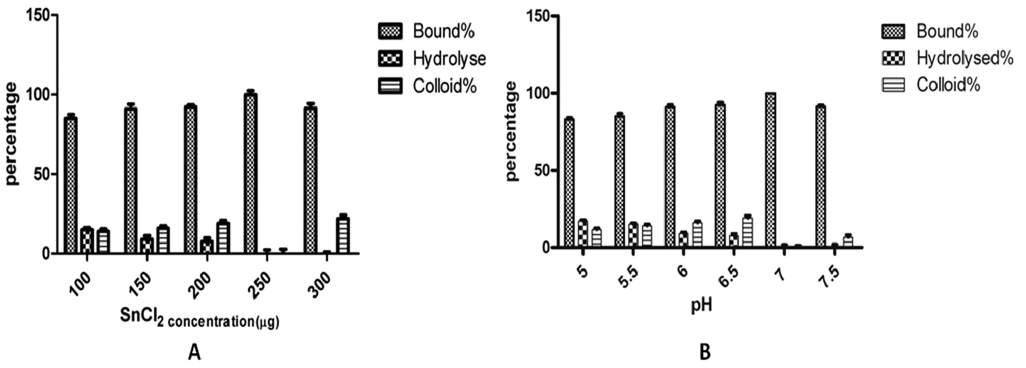

Figure 2. Variation of ^{99m}Tc labeling with stannous concentration (A) and pH (B).

datory to estimate the radiation doses to patients from administration of any novel radiopharmaceutical. Therefore, the effective dose for humans from [^{99m}Tc]Tc-DTPA-bis-(ChoEA) based on the biodistribution data in mice has also been estimated.

RESULTS

Chemistry and Radiochemistry. The schematic representation of the reaction is depicted in Scheme 1.

DTPA-bis(ChoEA) was obtained in 65% yield. The formation of the product was confirmed by ^{1}H, ^{13}C NMR, and mass spectroscopic analysis (see the Supporting Information). Spectroscopic analysis confirmed the formation of a pure single species, and thus, DTPA-bis(ChoEA) was directly utilized for radiolabeling and in vitro and in vivo studies. Rhenium complexation was done to validate the complexation of ^{99m}Tc with DTPA-bis(ChoEA). A significant difference was observed in the IR spectra of DTPA-bis(ChoEA) and Re-DTPA-bis(ChoEA). A strong shift was observed for the DTPA-bis(ChoEA) peak−C═O stretch of the acid at 1751.71 cm^{-1} and the −C═O stretch of the amide at 1621.29 cm^{-1} in the Re-DTPA-bis(ChoEA) complex. The probable −ReO peak was observed at 1564.77 cm^{-1} and −CH− stretch at 1403.85 cm^{-1}. Re-DTPA-bis(ChoEA) was characterized by HRMS, and m/z peaks were observed (see Supporting Information Figures S12 and S13).

Cell Viability. The cell viability for DTPA-bis(ChoEA) was evaluated by calculating the total surviving cell fraction for a range of concentrations (0.001−1000 μM). Toxicity was evaluated for the HEK-293 cell line for the unlabeled compound. The derivative was not able to induce cytotoxicity at lower concentrations. Both time- and concentration-dependent toxicities in the form of a time-dependent bar graph are shown in Supporting Information Figure S15. The conjugate was found to be relatively less toxic up to 100 μM concentrations, but a fall in the cell survival was observed at higher concentrations. The compound was observed to be nontoxic at 24 and 48 h at ≤100 μM concentrations. A

https://doi.org/10.1021/acsomega.1c04256
ACS Omega 2022, 7, 12509−12523

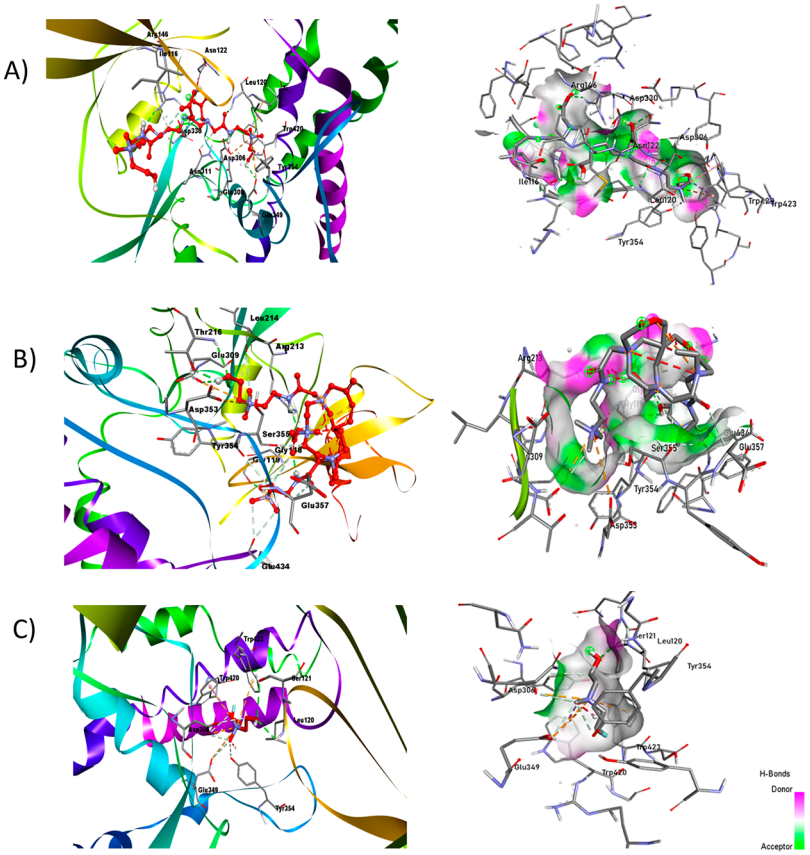

Figure 3. In silico-docked complex of the ligand with human choline kinase (PDB ID: 2CKQ). The ligand is represented by the ball and stick, while the target is ribbon-shaped and on the scale of hydrogen of (A) DTPA-bis-ChoEA, (B) [^{99m}Tc]Tc-DTPA-bis(ChoEA), and (C) fluoroethylcholine.

surviving fraction of 0.81 ± 0.05 was observed at 100 μM, 48 h; upon increasing the treatment concentration to 1000 μM, the 48 h surviving fraction observed was 0.44 ± 0.03. The compound did show toxicity at 1000 μM concentration at 48 and 72 h. The IC_{50} value was observed to be 500 μM.

Radiolabeling and Serum Stability Studies. A decay-corrected radiochemical yield of 98.5 ± 0.7% was obtained within 30 min with a minimal colloidal and hydrolyzed fraction. ^{99m}Tc radiolabeling was carried out for DTPA-bis(ChoEA) at room temperature using $SnCl_2$ as the reducing agent at pH 7. More than 98% radiochemical yield with minimal free, hydrolyzed, and colloidal fraction was observed for the DTPA conjugate without purification (Figure 2). The radiolabeled DTPA-bis(ChoEA) showed high kinetic inertness under physiological conditions. Very slow degradation of the complex was observed at 24 h. Approximately 97% of the radioconjugate was found to be intact at 24 h both in human serum and PBS (Supporting Information Figure S16). The results were suggestive of minimal trans-complexation of the chelate.

Theoretical Evidence of Binding of DTPA-Bis(ChoEA) to Choline Kinase. The target molecule used was the crystal structure of choline kinase complexed with phosphocholine (PDB ID: 2CKQ)[32] with a resolution of 2.4 Å. The target molecule was refined through AutoDock tools 4.2.[33] The characterization of the choline kinase crystal structure provides a way to study the binding interactions of the designed molecules for superior diagnostic and therapeutic efficacy for various cancer types. Docking studies were carried out for DTPA-bis(ChoEA), choline, and [^{99m}Tc]Tc-DTPA-bis(ChoEA) with choline kinase at the active sites. The results obtained through molecular modeling were used for analyzing the binding mode of the ligands to the active site of the protein (PDB ID: 2CKQ) (Figure S17). The two-dimensional representation of interaction in Figure 3 shows good binding of [^{99m}Tc]Tc-DTPA-bis(ChoEA) at the active binding site in two different conformations with one of the choline moieties binding at the substrate binding loop. The *G* score of −6.1 signifies dominant hydrogen bond interactions to the side chains and backbone residues (Leu214, Arg213, Thr216, Tyr354, Ser355, and Gly118) with the carbonyl and carboxylate groups in the ligand and −NH group showing charged interactions at Glu 349 and Asp306. Similarly, fluoroethyl choline with a *G*-score of −4.3 was found to be at the substrate binding site with hydrogen bond interactions with the side chains and residues (Gly119, Glu349, Tyr333, Tyr354, Trp420, Trp423, and Tyr440). The bivalent nature of DTPA-bis(ChoEA) depicts enhanced binding as compared to that of fluoroethyl choline. The docking results showed the potential of DTPA-bis(ChoEA) and [^{99m}Tc]Tc-DTPA-bis(ChoEA) being the substrate for choline kinase and thereby being effective for tumor targeting (Supporting Information Table S2).

Cell Binding Assay. The ability of [^{99m}Tc]Tc-DTPA-bis(ChoEA) to bind to the targeted enzyme choline kinase overexpressed in the prostate, colon, and lung cancer cells was evaluated on PC3, HCT116, and A549 cell lines, respectively. Nonspecific binding of the conjugates was assessed by the

https://doi.org/10.1021/acsomega.1c04256
ACS Omega 2022, 7, 12509−12523

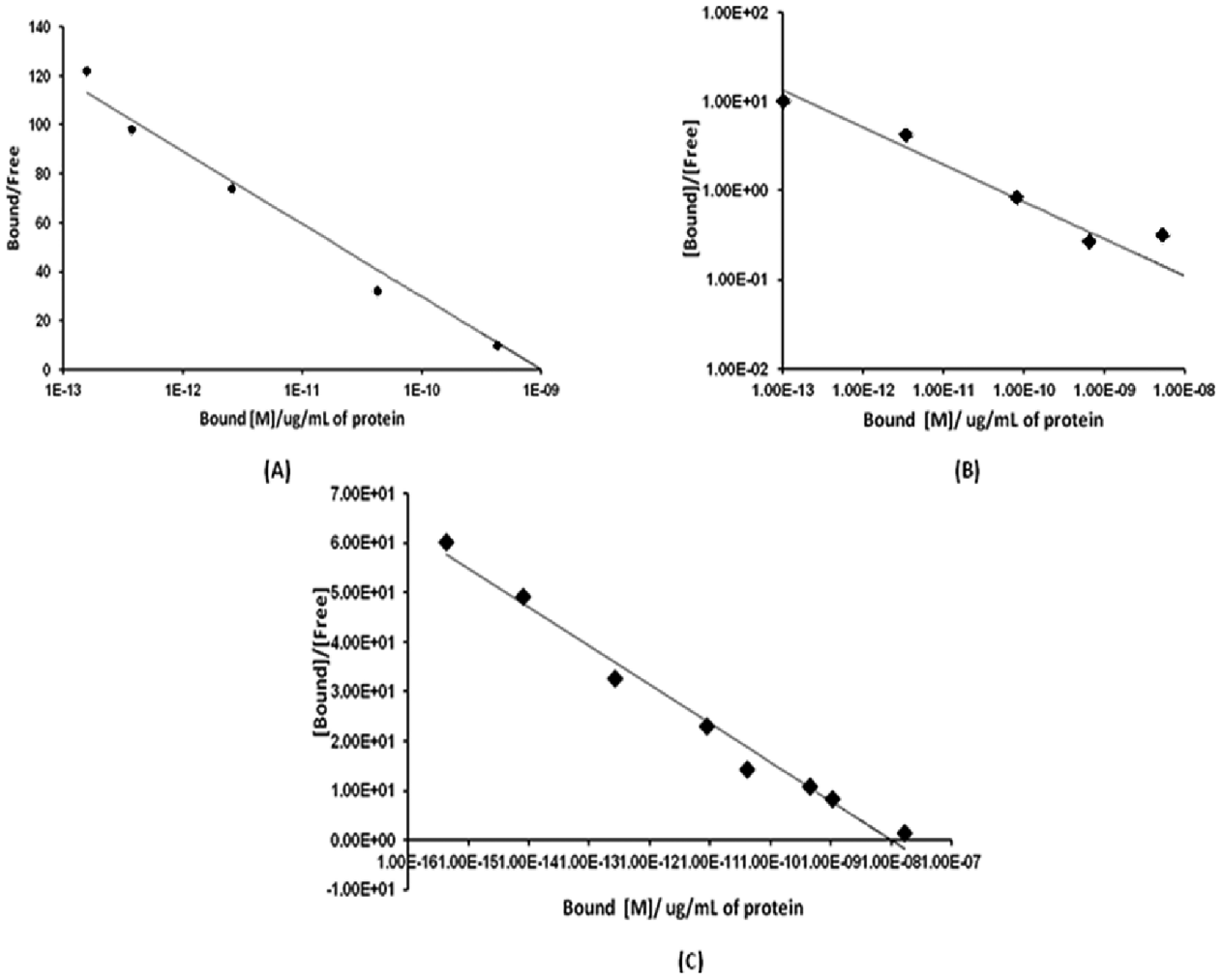

Figure 4. Cell binding assay for [^{99m}Tc]Tc-DTPA-bis(ChoEA) on (A) PC3 cells, (B) A549 cells, and (C) HCT116 cells. Representative Scatchard plot from the competitive binding assay for ^{99m}Tc-DTPA-bis-choline. Average value was plotted, wherein the SD was <2% in all cases.

saturation binding assay by adding 100-fold excess of unlabeled choline to the cells. Examination of the binding curve showed significant external binding of [^{99m}Tc]Tc-DTPA-bis(ChoEA). Figure 4A−C shows the Scatchard plots of the labeled conjugate on the PC3, A549, and HCT116 cell lines. The Scatchard plot depicts the affinity of [^{99m}Tc]Tc-DTPA-bis(ChoEA) to various choline kinase-overexpressed tumor cells. The K_d value was calculated and was found to be 5.35 pM, 0.621 nM, and 0.575 nM for the PC3, A549, and HCT116 cells, respectively. The B_{max} value for the PC3 cell line was determined to be 28.06 μM with a hill slope of 1.156, suggestive of two recognition binding motifs with enhanced affinity. The B_{max} value for the HCT116 cells was 1.2 μM with a hill slope of 1.11. The B_{max} value for A549 was found to be 7.09 μM with a hill slope of 1.089. Thus, the choline kinase/choline transporter expression was found to be in the order PC3 > HCT116 > A549.

In Vivo Toxicity Studies. It was observed that doses up to 500 mg/kg body weights were well tolerated (Supporting Information Figure S16) by the subjects without any visible side effect such as tremors and death. No adverse effects such as weight loss or mortality were observed in all groups up to 4 weeks after the intravenous administration of unlabeled conjugates.

In the initial phase when the mice were treated with 10, 100, and 1000 mg/kg body weight doses intravenously, no mortality was observed. In the second phase of toxicity evaluation, doses up to 1600 and 2900 mg/kg body weight were well tolerated with no visible sign of toxicity. The LD50 value was determined to be 3300 mg/kg body weight for intravenous administration.

Blood Kinetic Studies. For [^{99m}Tc]Tc-DTPA-bis(ChoEA), it was observed that 15.5 ± 1.4% of activity remained in circulation after 30 min of intravenous injection, as depicted in Figure 5. The conjugate showed a fast clearance from the blood pool with only 1.2 ± 0.53% of activity remaining at 6 h. At 24 h, only 0.36 ± 0.2% of activity remained in the blood. The biological half-life calculated was $T_{1/2}$ fast: 22.1 ± 1.2 min and $T_{1/2}$ slow: 14.6 ± 1.8 h. The blood clearance followed a biphasic pattern with a rapidly clearing initial phase followed by a slow phase.

Small-Animal Imaging. Comparative imaging and biodistribution studies of [^{18}F]F-FECH and [^{99m}Tc]Tc-DTPA-bis(ChoEA) demonstrated the liver and kidneys as the primary uptake sites for both the radiopharmaceuticals, as shown in Figure 6A,B. Both ^{18}F-FECH and [^{99m}Tc]Tc-DTPA-bis(ChoEA) demonstrated comparable biodistribution (Figure 6C). Reconstructed and processed CT-fused images generated from small-animal MicroSPECT/CT experiments performed

https://doi.org/10.1021/acsomega.1c04256
ACS Omega 2022, 7, 12509−12523

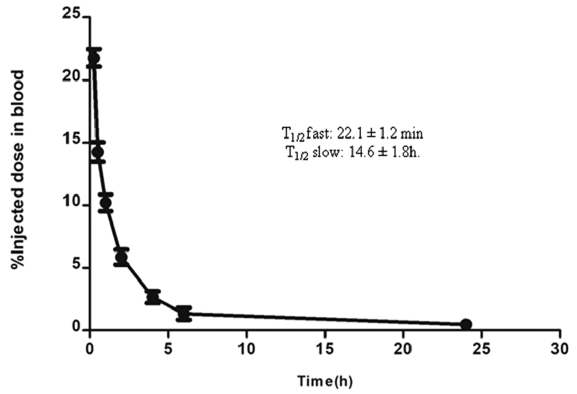

Figure 5. Blood kinetics of [^{99m}Tc]-DTPA-bis(ChoEA) in healthy mice (n = 5).

in PC3, A549, and HCT116 xenografted athymic mouse models 1 h after injections of [^{99m}Tc]Tc-DTPA-bis(ChoEA) are shown in Figures 7A, 8A, and 9A. 1 h of dynamic imaging was carried out to observe the tissue kinetics of [^{99m}Tc]Tc-DTPA-bis(ChoEA). The tumors were clearly visible with high contrast as compared to contralateral tissue contrast. The uptake pattern of [^{99m}Tc]Tc-DTPA-bis(ChoEA) in the organs except for tumors was similar in all three models. Data revealed both hepatobiliary and renal routes of excretion. The high liver and gall bladder activity depicts the hepatobiliary route as the primary route of excretion. The observed results were concomitant with the results obtained in the biodistribution or tissue distribution experiments of the radioconjugate. The highest tumor uptake was observed for the PC3 tumor models as compared to A549 and HCT116. The images were analyzed semiquantitatively by volumetric ROI analysis using AMIRA 4.1.1 image-processing software (Supporting Information Table S2). The ROI analysis depicts the tumor/muscle ratios

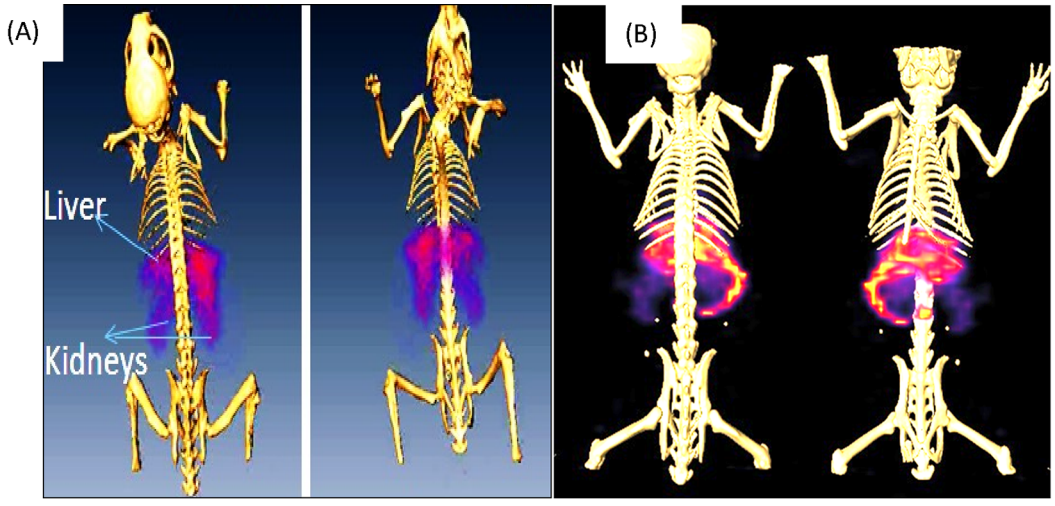

(C)

Organ	^{18}F-FECH (10min)	^{18}F-FECH (30min)	^{18}F-FECH (60min)	^{99m}Tc-DTPA-bis(ChoEA) (10min)	^{99m}Tc-DTPA-bis(ChoEA) (30min)	^{99m}Tc-DTPA-bis(ChoEA) (60min)
Blood	2.306±0.040	1.933±0.200	0.045±0.006	3.049 ±0.015	1.628±0.011	0.050±0.021
Heart	0.117±0.010	0.132±0.050	0.092±0.002	0.091±0.020	0.141±0.021	0.063±0.010
Brain	0.290±0.050	0.018±0.010	0.009±0.002	0.305±0.001	0.187±0.001	0.016±0.004
Lungs	0.093±0.020	0.171±0.032	0.224±0.031	0.143±0.070	0.221±0.091	0.030±0.006
Liver	3.512±0.221	4.601±0.120	2.940±0.110	2.832±0.110	3.180±0.142	2.211±0.100
Spleen	0.023±0.010	0.017±0.002	0.011±0.008	0.053±0.018	0.031±0.011	0.012±0.010
Kidney	1.841±0.210	1.672±0.120	1.481±0.190	0.991±0.158	0.812±0.095	0.517±0.160
Muscle	0.040±0.020	0.020±0.010	0.010±0.010	0.010±0.011	0.011±0.050	0.007±0.090
Bone	0.093±0.020	0.071±0.015	0.024±0.010	0.013±0.005	0.021±0.008	0.010±0.004

Figure 6. (A) MicroPET/CT-fused image of [^{18}F]F-FECH. (B) MicroSPECT/CT-fused image of [^{99m}Tc]Tc-DTPA-bis(ChoEA). (C) Table showing the comparative biodistribution of [^{18}F]F-FECH and [^{99m}Tc]Tc-DTPA-bis(ChoEA) in healthy BALB/c mice.

https://doi.org/10.1021/acsomega.1c04256
ACS Omega 2022, 7, 12509−12523

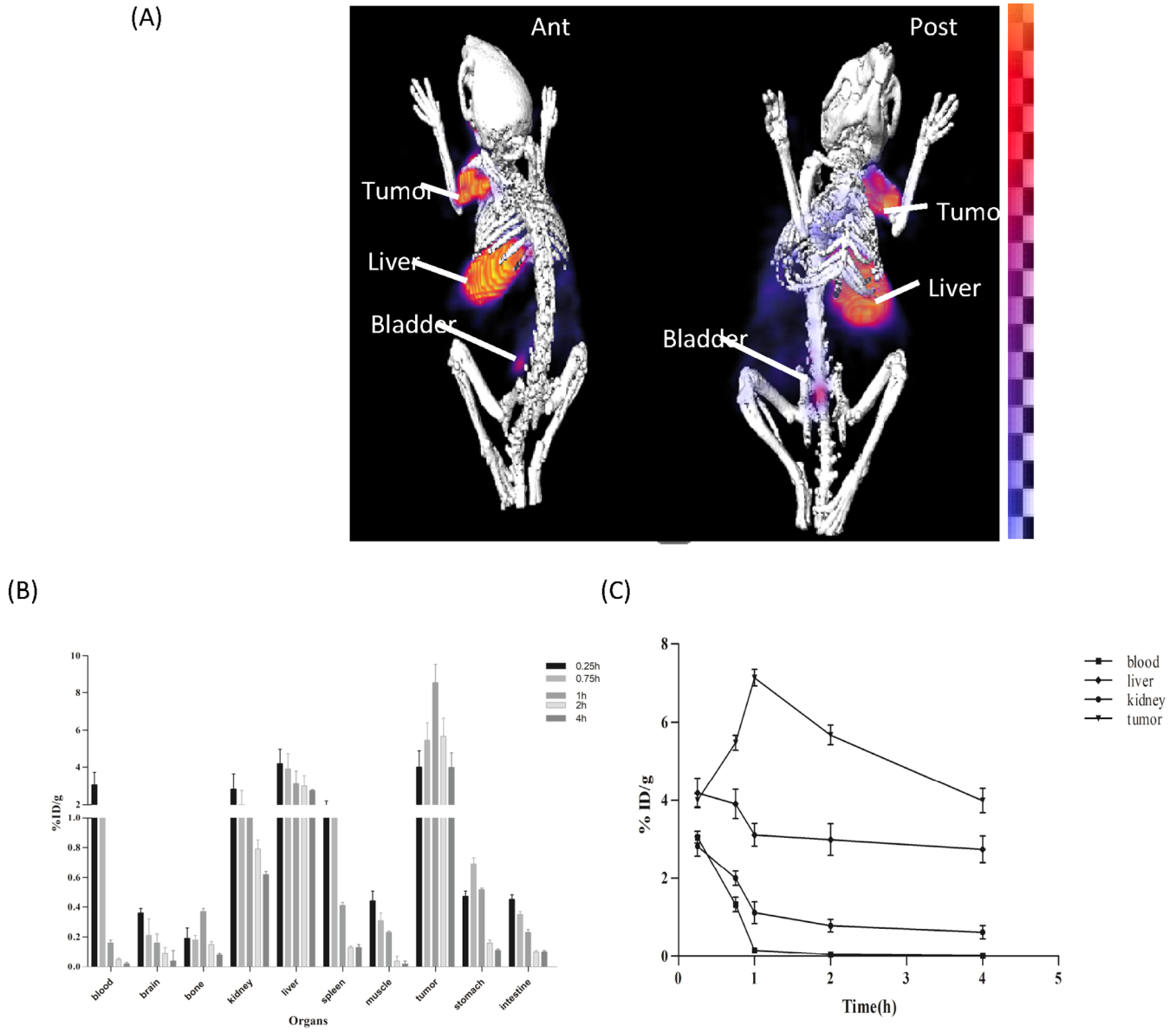

Figure 7. In vivo scintigraphy and biodistribution of [^{99m}Tc]Tc-DTPA-bis(ChoEA) on PC3 athymic mouse models. (A) MicroSPECT/CT coregistered whole-body scan (anterior and posterior) 1 h after intravenous administration. (B) Bar graph representing the biodistribution of [^{99m}Tc]Tc-DTPA-bis(ChoEA) on athymic mice bearing PC3 tumors. (C) Kinetics of [^{99m}Tc]Tc-DTPA-bis(ChoEA) in PC3 mouse models.

of 36.58 ± 4.5, 29.90 ± 5.12, and 34.22 ± 5.2 in PC3, A549, and HCT116, respectively. The images were suggestive of a high target-to-nontarget ratio. Imaging studies clearly revealed high tumor uptake with an appreciable tumor-to-muscle ratio perquisite for tumor imaging.

Tissue Distribution Studies. MicroSPECT imaging studies were further validated by tissue organ biodistribution studies. [^{99m}Tc]Tc-DTPA-bis(ChoEA) biodistribution studies were carried out in control mice, PC3, HCT116, and A549 tumor mouse models. [^{99m}Tc]Tc-DTPA-bis(ChoEA) showed both hepatobiliary and renal uptake. The initial pattern of biodistribution demonstrated blood pool activity, but at later intervals, all the activity cleared from the body. The distribution of the radioprobe in various tissue/organs was expressed as a percentage of injected dose per gram of organ weight (%ID/g) represented as a bar graph in Figures 7B, 8B, and 9B.

The maximum tumor accumulation in the PC3 mouse model was 8.9 ± 0.99 %ID/g, and the T/M ratio was 37.13 ± 5.57 after 1 h of intravenous injection; in the A549 and HCT116 mouse models, it was found to be 8.1 ± 1.1 and 7.98 ± 0.98 %ID/g with the T/M ratios of 29.36 ± 4.32 and 35.92 ± 4.96, respectively.

The time−activity curves depicted in Figures 7C, 8C, and 9C are plotted for the liver, kidneys, tumor, and blood for the PC3, A549, and HCT116 biodistribution studies.

A similar pattern of high tumor uptake with hepatic and renal uptake was observed in all cases. The liver and renal uptake demonstrated that the radioconjugate followed both renal and hepatobiliary routes of excretion. Initial blood pool activity with rapid clearance was also observed. A similar pattern of biodistribution with the liver and kidneys as the primary uptake sides was observed for [^{18}F]F-FECH biodistribution (Figure 6C).

https://doi.org/10.1021/acsomega.1c04256
ACS Omega 2022, 7, 12509−12523

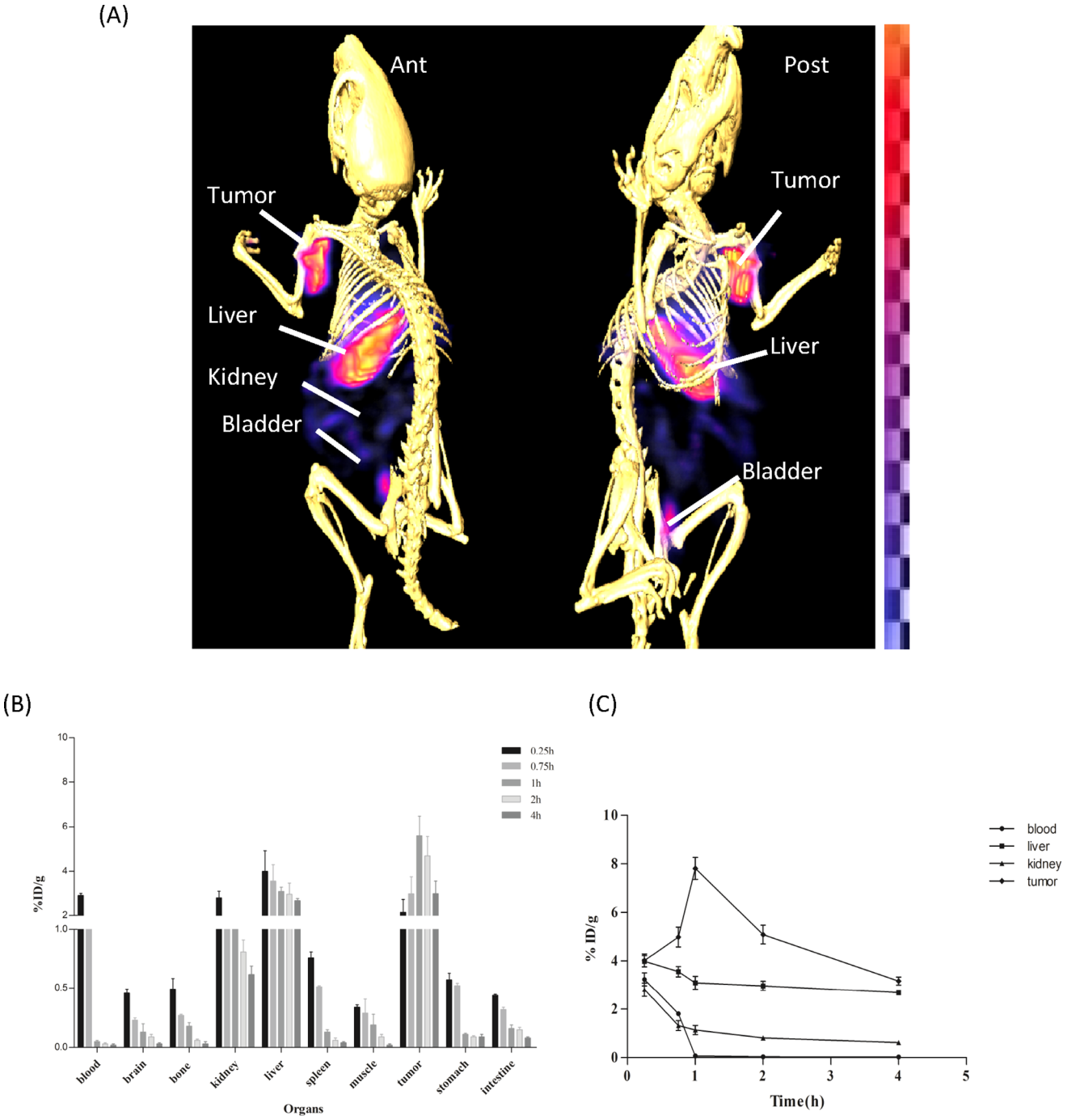

Figure 8. In vivo scintigraphy and biodistribution of [^{99m}Tc]Tc-DTPA-bis(ChoEA) on A549 athymic mouse models. (A) MicroSPECT/CT coregistered whole-body scan (anterior and posterior) 1 h after intravenous administration. (B) Bar graph representing the biodistribution of [^{99m}Tc]Tc-DTPA-bis(ChoEA) on athymic mice bearing A549 tumors. (C) Kinetics of [^{99m}Tc]Tc-DTPA-bis(ChoEA) in A549 mouse models.

Dosimetry. The residence time of [^{99m}Tc]Tc-DTPA-bis(ChoEA) in the control and athymic mice for 10 source organs was calculated, as shown in Table 1. The radiation dose estimates for a human weighing 70 kg from the mice biodistribution data are shown in Table 2.

The highest absorbed dose was in the bladder (0.0069 mSv/MBq). The effective dose was estimated to be 0.00467 mSv/MBq (4.67 mSv/GBq), resulting in a radiation dose of up to 1.73 mSv for the injection of [^{99m}Tc]Tc-DTPA-bis(ChoEA).

DISCUSSION

Choline and its analogues are well-established effective biomarkers for PET diagnostic applications as they efficiently demarcate the differences between malignant and normal cells. Various studies employing biochemical analysis and magnetic resonance spectroscopy have demonstrated elevated levels of choline and its metabolites such as phosphocholine and phosphoethanolamine under various malignant conditions.[34] Upregulated choline kinase activity in malignant cells provides a potential mechanism for the radiolabel choline analogue accumulation by neoplasms.[35]

https://doi.org/10.1021/acsomega.1c04256
ACS Omega 2022, 7, 12509−12523

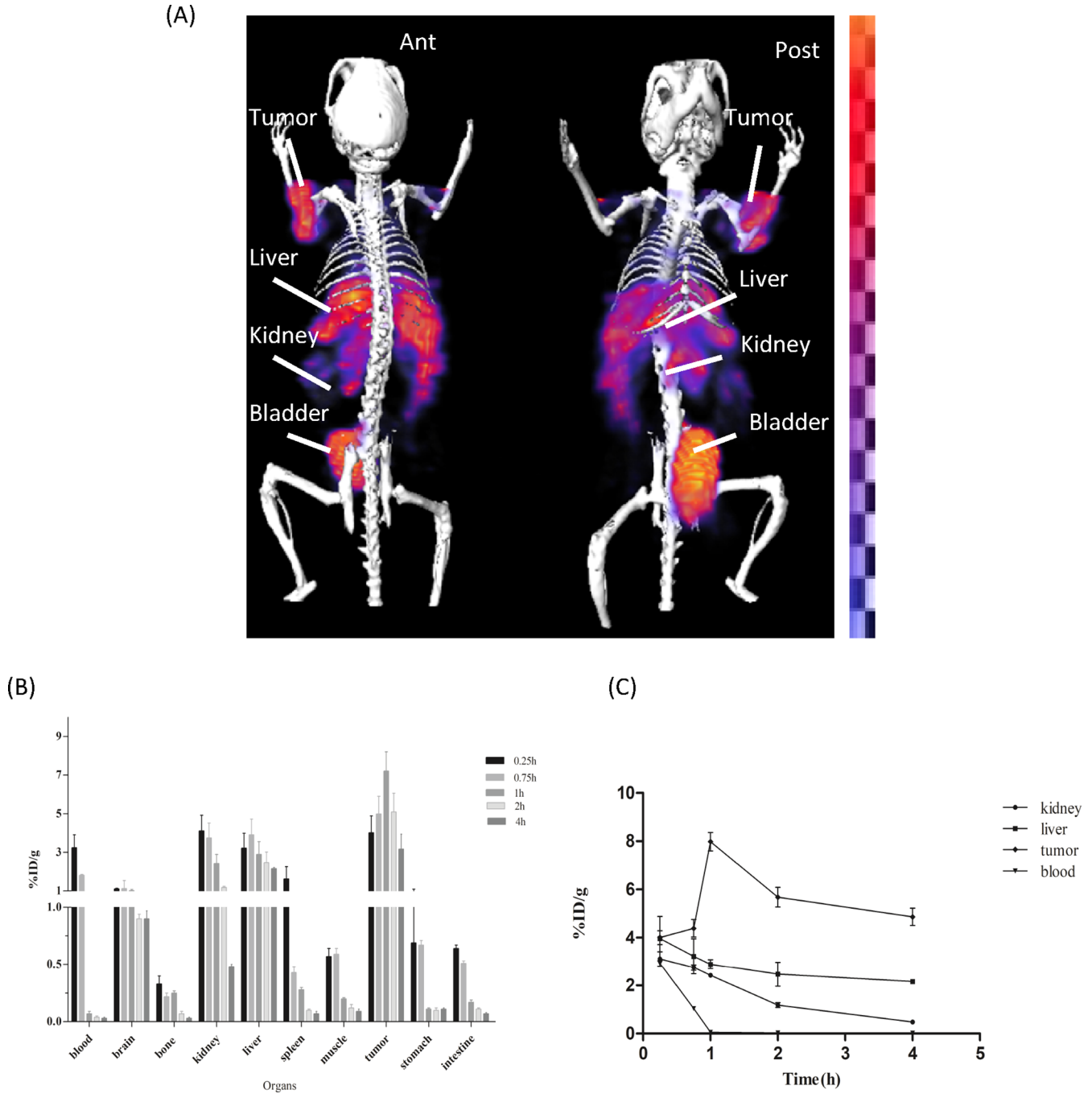

Figure 9. In vivo scintigraphy and biodistribution of [^{99m}Tc]Tc-DTPA-bis(ChoEA) on HCT 116 athymic mouse models. (A) MicroSPECT/CT coregistered whole-body scan (anterior and posterior) 1 h after intravenous administration. (B) Bar graph representing the biodistribution of [^{99m}Tc]Tc-DTPA-bis(ChoEA) on athymic mice bearing HCT116 tumors. (C) Kinetics of [^{99m}Tc]Tc-DTPA-bis(ChoEA) in HCT116 mouse models.

The selected choline system has attracted attention for its exploration as a possible target for noninvasive targeted imaging of tumors with altered choline metabolism. Hara and co-workers fruitfully introduced choline-based tracers for the visualization of brain and prostate tumors.[36,37] ^{11}C-choline, ^{18}F-fluoromethylcholine, and ^{18}F-fluoroethylcholine are well-known choline derivatives employed for PET imaging. Choline analogues such as ^{11}C-choline, ^{18}F-fluorocholine, and ^{18}F-fluoroethylcholine are markers of choline kinase overexpression and upregulated metabolism under oncological conditions.

Nevertheless, the shorter half-life of ^{11}C-labeled radiopharmaceuticals always imposes limitations of use in facilities with cyclotron availability. To overcome this limitation, ^{18}F-labeled conjugates have also been synthesized and reported as an alternative to [^{11}C]C-choline for brain and prostate imaging.[38,39] Due to the limited half-life of PET tracers, we have attempted to develop an efficient ^{99m}Tc-based choline derivative to overcome the limitation of half-life with an easy radiopharmacy and an acceptable resolution.

^{99m}Tc being a generator-based radioisotope has the advantage of single-step kit-based radiopharmacy over complex

https://doi.org/10.1021/acsomega.1c04256
ACS Omega 2022, 7, 12509−12523

Table 1. Residence Time (in Hours) of [^{99m}Tc]Tc-DTPA-Bis(ChoEA) for the Measured Organs and Rest of the Body

	residence time (h)	
source organs	control	PC3
heart	0.0017 ± 0.0002	0.0009 ± 0.0003
lungs	0.0149 ± 0.0021	0.0062 ± 0.0007
liver	0.0166 ± 0.0013	0.0808 ± 0.0032
spleen	0.0080 ± 0.0024	0.0008 ± 0.0001
kidneys	0.0200 ± 0.0027	0.0088 ± 0.0019
stomach	0.0019 ± 0.0007	0.0006 ± 0.0001
brain	0.0010 ± 0.0002	0.0125 ± 0.0073
intestines	0.0076 ± 0.0019	0.0015 ± 0.0004
rest of the body	8.3990 ± 0.0042	8.5130 ± 0.0037

Table 2. Absorbed Dose Estimates of [^{99m}Tc]Tc-DTPA-Bis(ChoEA) for the Target Organs in Humans Determined from Mouse Data[a]

target organ	absorbed dose (mGy/MBq)
adrenals	0.0052 ± 0.002
brain	0.0016 ± 0.001
breasts	0.0037 ± 0.012
gall bladder wall	0.0053 ± 0.003
lower large intestine wall	0.0061 ± 0.004
small intestine	0.0065 ± 0.012
stomach wall	0.0048 ± 0.001
upper large intestine wall	0.0061 ± 0.002
heart wall	0.0048 ± 0.001
kidneys	0.0040 ± 0.00
liver	0.0025 ± 0.001
lungs	0.0030 ± 0.001
muscles	0.0031 ± 0.001
ovaries	0.0063 ± 0.002
pancreas	0.0056 ± 0.012
red marrow	0.0043 ± 0.013
osteogenic cells	0.0124 ± 0.011
skin	0.0030 ± 0.002
spleen	0.0036 ± 0.0016
testes	0.0045 ± 0.022
thymus	0.0046 ± 0.027
thyroid	0.0048 ± 0.019
urinary bladder wall	0.0059 ± 0.032
uterus	0.0065 ± 0.042
total body	0.0040 ± 0.003
effective dose equivalent (mSv/MBq)	0.0054 ± 0.002
effective dose (mSv/MBq)	0.0047

[a]Data presented as mean ± S.D.

multistep approaches for the conjugation of cyclotron-based isotopes such as ^{18}F and ^{11}C.[40] DTPA was selected as a scaffold due to its fast complexation kinetics, and the *N*,*N*-dimethylated amine derivative of choline with increased lipophilicity was the selected biomarker for tracking choline kinase expression.

A variety of DTPA ligands are approved clinically for human use. Polyaminopolycarboxylate ligands are known for efficient coordination with ^{99m}Tc, thereby favoring a better radiolabeling of the vector. The bivalent approach followed for DTPA conjugation to vectors yields a more stable system and favors the desired effect. Also, the dimeric systems possess the ability of bridging independent recognition sites, which results in a thermodynamically favorable binding interaction as compared to monovalent binding for increasing the affinity toward the target.[41]

The bivalent ligand allows the desired effect to be achieved at very low concentrations with enhanced binding as compared to monovalent derivatives.[42] Various reports are suggestive of the application of DTPA-conjugated biomolecules for targeting specific enzymes, receptors, and so forth with high target specificity and selectivity. The synthetic approach involves quaternization of the dimethylethanolamine moiety, followed by its conjugation to DTPA-bis-anhydride. During synthesis, all the steps are stoichiometrically controlled to avoid the formation of monomer systems and undesired impurities. An appreciable yield of DTPA-bis-choline, 85%, was obtained by the synthetic approach followed. The synthesized [^{99m}Tc]Tc-DTPA-bis(ChoEA) moiety possesses favorable characteristics such as water solubility, low toxicity, and high stability requisites in clinical utilization. With rhenium as an analogue, technetium could be used as a useful tool to direct studies toward technetium complexation. In this regard, complexation with Re(III)Cl_3 was done to characterize the probable complexation with technetium.

Preclinical SPECT/CT studies were well supported by in vitro cell binding and ex vivo biodistribution experiments. The radioactivity accumulation at the tumor site was quite significant as compared to the contralateral tissue. The cell lines used in the present study were chosen as high phosphocholine levels are demonstrated in the metabolome of PC3 as compared to normal cells; these levels are primarily due to the overexpression of choline kinase.[43,44] The high mRNA expression level of choline kinase has been studied in the HCT116 cell line as well. ^{15}Choline transporters (ChT) have already been reported to be more preferentially expressed in A549 cancer cells as compared to noncancerous cells.[20,21] For human clinical applications, it is important to weigh the risk versus benefit from any medical radiation exposure. In nuclear medicine procedures, the dosimetry study is required before any clinical administration of a radiopharmaceutical, which helps in the determination of the activity range. Accordingly, it becomes mandatory to estimate the radiation doses to patients from the administration of any novel radiopharmaceutical. We estimated the effective dose to humans from [^{99m}Tc]Tc-DTPA-bis(ChoEA) based on the biodistribution data in mice. Preclinical dosimetry data demonstrated the safe use of the radiopharmaceutical as it was comparable to most widely ^{99m}Tc radiopharmaceuticals.[45]

A wide range of choline analogues for PET have been reported in the literature as valuable imaging probes for the diagnosis of various neoplastic conditions of the prostate, cervix, lungs, breast, brain, and so forth. In the past few years, ^{68}Ga-labeled PSMA analogues with high specificity than choline analogues have been introduced clinically for prostate cancer detection specifically, but these PSMA analogues are not widely available and also have few drawbacks such as masking of prostate tumor lesions in or nearby high-background regions, false negative scans due to low PSMA expression, and so forth as such radiolabeled choline analogues only support the detection of prostate tumors.[46−49]

We have reported a DTPA-conjugated cholineethylamine derivative in a preliminary form for SPECT applications, which can be easily translated and amended into routine clinical practice. The dianhydride derivative of DTPA employed as chelator facilitates the formation of a complex with a single

https://doi.org/10.1021/acsomega.1c04256
ACS Omega 2022, 7, 12509−12523

ligand per metal atom, the requisite for in vivo stability and for biological activity.

Rapid clearance with a low nontargeted accumulation and significant target uptake and dosimetry correlation with already reported [^{99m}Tc]Tc-DTPA, which is a clinically accepted radiotracer for nuclear medicine imaging makes it an acceptable system that can be easily translated to clinical applications. The first in-human clinical study was done in a biochemically and symptomatically known untreated subject of prostate cancer after the intravenous injection of [^{99m}Tc]Tc-DTPA-bis(ChoEA) (0.016 mg/kg) without bladder irrigation (Supporting Information Figure S19). Maximum activity was observed in the kidneys and liver, no radioactivity was found in the bones, neither in the bone marrow nor in the epiphysis in the whole-body SPECT scan. The region of the prostate appeared to be obscured by renal tracer activity. Although the initial scan showed rapid accumulation at the target site, it needs further intervention. Kidneys possess high choline kinase activity owing to the high tracer activity of choline analogues.[50] The renal accumulation of [^{99m}Tc]Tc-DTPA-bis(ChoEA) in contrast to ^{11}C choline may impose a limitation for pelvic imaging, which can be overcome by bladder irrigation using a urinary catheter to eliminate bladder radioactivity. This method of bladder irrigation for clinical imaging has been successfully reported by Hara and co-workers.[26] The synthetic approach requires only a skilled radiochemist and an airtight working environment as compared to extensive radiochemistry associated with cyclotron-based analogues. Also, the shorter half-life associated with PET isotopes limits the transportation of radio-probes, which can be easily overcome using ^{99m}Tc, which also facilitates the long-term study of the subject. Hence, the preclinical results obtained are suggestive of [^{99m}Tc]Tc-DTPA-bis(ChoEA) as a promising candidate for tumor imaging, which does not require any complex radiochemistry with high radiochemical yield, high stability, minimal toxicity, and a high target-to-nontarget ratio supporting an easy translation to clinical use. As diagnostic intervention paves the way for therapeutics, choline transporters and choline kinase are important targets for developing therapeutic and preventive probes for cancer. Future studies with ^{177}Lu warrant its application as a delivery system for therapeutic radioisotopes for selective and specific tumors.

CONCLUSIONS

Upregulated choline metabolism and choline kinase activity have motivated the development of choline analogues for imaging neoplasm. Thus, a choline derivative can be a good candidate for imaging choline-overexpressed tumors and their prognostications. In the present work, DTPA-bis(ChoEA), a bivalent, homodimer choline-based system has been developed and bioevaluated for its role in the diagnosis of various tumors with already reported choline overexpression. Preclinical findings of DTPA-bis(ChoEA) have demonstrated its potential as an imaging probe in terms of its stable and defined radiochemistry with ^{99m}Tc. In preclinical models, [^{99m}Tc]Tc-DTPA-bis(ChoEA) shows high and target-specific accumulation. The synthesized moiety DTPA-bis(ChoEA), a homodimeric system, not only provides a cost-effective alternative to choline-based PET analogues but also increases the selectivity of phosphorylation. The unlabeled bivalent ligand also shows high affinity and specificity toward choline kinase. Furthermore, the application of DTPA-bis(ChoEA) can be extended with $^{67/68}$Ga, thereby facilitating the versatility for imaging using both SPECT and PET. These findings sufficiently encourage the utilization of [^{99m}Tc]Tc-DTPA-bis(ChoEA) as an oncologic SPECT tracer for imaging various choline-overexpressed tumors with high specificity for clinical applications.

MATERIALS AND METHODS

Chemicals. Analytical-grade reagents were procured from Merck Specialties Pvt. Limited. Instant thin-layer chromatography strips (ITLC-SG) were obtained from Paul Gelman, USA. ^{99m}Tc was procured from the in-house Regional Centre for Radiopharmaceuticals (Northern Region), Board of Radiation Isotopes and Technology, Department of Atomic Energy, India.

Instrumentation. Mass spectra and ESI-MS in positive and negative modes were generated using an in-house Agilent 6310 system ion trap. Proton and carbon NMR spectra too were acquired using an in-house Bruker ADVANCE II spectrometer (^{1}H NMR and ^{13}C NMR, 400 and 100 Hz). A well-type calibrated Capintec Gamma counter was used for radiolabeling counting. The MTT assay absorbance was acquired using a BioTek Synergy H4 hybrid multiplate reader. MicroSPECT acquisitions were performed using a GE_FLEX Triumph MicroPET/SPECT/CT triple-modality system. HRMS was done using a Thermo Scientific Q Exactive Plus Hybrid Quadrupole-Orbitrap mass spectrometer.

Ethical Statement. All the protocols employed for animal experiments were approved by the institutional ethical committee (CPCSEA Regn no. 8/GO/RBi/S/99). As per the UKCCCR guidelines,[30] for animal welfare in experimental neoplasia to avoid unnecessary tumor burden to the subject, a tumor volume not more than 100 mm^3 was used and animals were sacrificed by the cervical dislocation method. All the experiments involving radioactive materials were carried out under the authorization of the radiation safety commission in accordance with the Institutional Nuclear Regulatory Commission license.

Cell Culture. A549 (human NSCLC epithelial cell line), HCT116 (human colon cancer cell line), and PC3 (human prostate cancer cell line) were obtained from NCCS, Pune, India. All the cells were maintained in their respective media containing fetal bovine serum (FBS). The cells were prescreened for mycoplasma contamination (MycoFluor Mycoplasma Detection Kit, Thermo Fisher Scientific) and their ability to form tumors <1000 cells in mice before the start of experiment. The A549 and PC3 cells were cultured and maintained in DMEM F12 (Sigma-Aldrich), supplemented with 7.5% sodium bicarbonate (w/v) (Invitrogen, Carlsbad, CA), 10% FBS, and 1% penicillin−streptomycin (Invitrogen). The HCT116 cell line was cultured in high-glucose DMEM (Sigma-Aldrich). All cell lines were maintained at 37 °C and 5% CO_2, equilibrated with atmospheric O_2 in a humidified incubator containing 20% O_2 unless otherwise stated.

Ligand Synthesis and Characterization. Quaternization of dimethylaminoethanol was carried out in four steps (Scheme 1). The final product was characterized by mass and NMR spectroscopy (details provided in the Supporting Information).

Step 1: Synthesis of 2-(dimethylamino)ethylacetate (A): A 1:1 mixture of *N*,*N*-dimethylethanolamine and acetic anhydride was stirred at 0 °C overnight. The pH of the reaction mixture was neutralized to 7 using a 0.5 M sodium bicarbonate solution. The organic layer was collected by extraction with

https://doi.org/10.1021/acsomega.1c04256
ACS Omega 2022, 7, 12509−12523

dichloromethane, which was further dried over anhydrous sodium sulfate and evaporated under reduced pressure to obtain the crude product. The crude product was then subjected to column chromatography on silica gel with 8.5:1.5 dichloromethane/methanol as the eluent system to obtain the desired product as a pale yellow oil (75%). Step 2: Synthesis of 2-acetoxy-*N*-(2-aminoethyl)-*N*,*N*-dimethylethanaminium (B): To A (5 mmol) in acetonitrile (30 mL), bromoethylamine hydrobromide (7.5 mmol) was added under inert conditions, and the reaction mixture was refluxed for 16 h. The mixture was then cooled to room temperature and evaporated to dryness under vacuum conditions to obtain the crude product. The crude product was washed thrice with DCM to remove unwanted impurities (Supporting Information Figures S14 and S15).

Step 3: Synthesis of 2-amino-*N*-(2-hydroxyethyl)-*N*,*N*-dimethylethanaminium (C): To B (2.85 mmol) in anhydrous methanol, potassium bicarbonate (3.42 mmol) was added and stirred at 0 °C overnight and then quenched with a saturated aqueous ammonium chloride solution. The final product was obtained by extraction with ethylacetate. The solvent was evaporated to dryness with methanol under vacuum to obtain the crude product. The product was washed thrice with chloroform. Addition of ice-cold diethylether led to the formation of a pure product.

Step 4: Synthesis of 6,9,12-tris(carboxymethyl)-N^1,N^{17}-bis(2-hydroxyethyl)-N^1,N^1,N^{17},N^{17}-tetramethyl-4,14-dioxo-3,6,9,12,15-pentaazaheptadecane-1,17-diaminium (D): To C (1.5 mmol) in 10 mL of dry DMF under inert conditions was added 0.429 mmol DTPA-anhydride and 4.2 mmol triethylamine. The reaction mixture was refluxed for 16 h and then stirred for 48 h at room temperature. The filtrate was precipitated out, DMF was reduced under vacuum, and acetone was added. The pure compound was obtained as a pale-yellow precipitate. The final product was well characterized by NMR and MS (Supporting Information Figures S1–S11).

MTT Assay/Cell Viability Assay. The exponentially growing cells were seeded 24 h prior to treatment in a 96-well microtiter plate with a cell density of 4000 cells per well. The cells were treated with varying concentrations of unlabeled DTPA-bis(cholineethylamine) for different time intervals (ranging from 24 to 72 h). At the end of the treatment, both the treated and untreated cells were subjected to incubation with MTT at a concentration of 0.1 mg/mL for 3 h at 37 °C, and the medium was removed subsequently. The cells from each treated well were lysed, and formazan crystals were dissolved in 150 μL of DMSO and incubated for 30 min. The optical densities of the extracts were recorded (reference filter: 630 nm). The surviving fractions were evaluated and were plotted against the concentration as a function of time.[52]

Preparation of the Rhenium Complex. The structure of radiolabeled DTPA-bis(cholineethylamine) was established using rhenium(III)chloride [$Re(III)Cl_3$]. The surrogate rhenium complex of [^{99m}Tc]Tc-DTPA-bis(ChoEA) was prepared. Equimolar concentrations of rhenium(III) chloride (4.6 mg; 16.05 μmoL) and 10 mg of the unlabeled DTPA-bis(cholineethylamine) precursor were dissolved in 0.5 M sodium acetate (1 mL). The reaction mixture was then heated at 90 °C for 2 h at pH 6.5. Visible conversion of the blackish-brown solution to a pale-yellow solution was observed. The Re–DTPA–bis(cholineethylamine) complex was characterized by IR and high-resolution accurate MS (see Supporting Information Figures S12 and S13). The calculated and observed mass in the HRMS spectra of the plausible Re–DTPA–bis(ChoEA) complex is shown in Table S1.

Radiolabeling and Serum Stability. A standard procedure of radiolabeling using stannous chloride as the reducing agent was employed for radiolabeling. Stability of the radioprobe was analyzed both in human serum and PBS. Radiolabeling of the conjugate was carried out at room temperature using 1 mg of DTPA-bis(ChoEA) dissolved in 500 μL of water and 300 μL of stannous chloride (1 mg/mL in 10% acetic acid) as the reducing agent at pH 7 using 0.1 M Na_2CO_3. The radiochemical purity was assessed using the ascending ITLC-SG strips using 100% acetone, 100% saline, and pyridine/acetic acid/water (3:5:1.5) as the solvent fronts. Serum stability of the complexes was also analyzed both in human serum and 0.1 M pH 7.4 PBS at different intervals of time for 24 h. For human serum stability, blood samples were withdrawn from healthy volunteers with consent and allowed to clot for 1 h at 37 °C, and serum was separated. 100 μL of the radiolabeled complex was added to 900 μL of human serum and incubated. The percentage dissociation of the conjugates was determined using the ITLC-SG method from the 0 to 24 h time interval. In PBS, 100 μL of the compound was directly incubated with 900 μL of PBS and monitored using ITLC-SG for 24 h. [^{18}F]-FECH was produced in an in-house cyclotron facility using automated MX TracerLab GE, 16.5 MeV Cyclotron.

In Silico Docking Studies. As the choline kinase structure was a dimer, chain A was taken into consideration for study. Modeling of the ligand was carried out through ChemDraw software, and its energy minimization and 3D coordinates were generated through open Babel software.[51] The docking study was performed by AutoDock Vina[52] and was analyzed using the BIOVIA Discovery Studio visualizer.[53] The best pose was generated based on the rank.

Cell Binding Assay. The binding experiments were carried out to examine the specificity of radiolabeled DTPA-bis(ChoEA) to bind externally on tumor cells. The binding studies were carried out on PC3, A549, and HCT116 cell lines, already reported for high choline transporters and choline kinase expression. The cells were washed twice with PBS and resuspended in 1 mL of PBS. The experiments were performed at 37 °C. The cells were treated with an increasing concentration from 0.01 nM to 10 μM radioligands and incubated for 30 min in the presence and absence of 100-fold excess of the competitor (unlabeled choline) to estimate the nonspecific and total binding, respectively. After incubation, the cells were washed four times with ice-cold PBS. Finally, the cells were lysed and cell-bound radioactivity was determined using a gamma scintillation counter. The total protein content of the lysed cells was determined by the bicinchoninic acid method. The Scatchard plot was then generated to calculate the K_d and B_{max} values.

Experimental Animals. Male BALB/c mice 6–8 weeks old (27 ± 3 g) and athymic mice (25 ± 3 g), 4–6 weeks old, kept in a pathogen-free environment, maintained on sterile diet and water ad libitum, were employed in the experiments. Athymic male mice were inoculated with A549, HCT116, and PC3 human tumor cell lines. 5×10^6 cells in 0.1 mL (PBS) of the cell suspension of the respective cell lines were inoculated subcutaneously in the forelimb of the mice. The tumor volume was monitored on a regular basis until it reached 100 mm^3. The tumor dimensions were measured using a caliper, and the

https://doi.org/10.1021/acsomega.1c04256
ACS Omega 2022, 7, 12509–12523

tumor volume was calculated using a standard formula, that is, tumor volume = $S^2 \times L/2$, where S and L correspond to the measured smallest and largest tumor diameter. 2% isoflurane in 2 L/min oxygen on-bed inhalation was employed for anesthesia during the imaging experiments.

Animal Toxicity Studies. The animal toxicity studies were carried out in BALB/c mice. A single dose of DTPA-bis-(ChoEA) dissolved in normal saline at pH 7 was administered intravenously through the tail vein in different groups of six mice each along with the control group. The dosage levels were 50−500 mg/kg body weight. The animals were weighed weekly and observed for any signs of toxicity and mortality after treatment. The lethal dose (LD50) for DTPA-bis-(ChoEA) was calculated by Lorke's method. In the first phase, male and female BALB/c weighing 25−30 g were divided into three groups of three mice each. The animals were treated with 10, 100, and 1000 mg/kg body weight doses of DTPA-bis(ChoEA) (dissolved in PBS) through the tail vein. The animals were observed for 24 h for any signs of toxicity and mortality. In the second phase of toxicity evaluation, the animals were divided into three groups of five mice each. In this phase, the animals were treated with doses of 1600, 2900, and 5000 mg/kg body weight through the tail vein and were observed for 14 days post-treatment. Any sign of toxicity and mortality was recorded. The median lethal dose was calculated in the second phase.

Blood Kinetic Studies. For blood kinetic evaluation, 10 MBq of the radiolabeled complex was injected through the tail vein of the mice. At different time intervals from 5 min to 24 h after intravenous administration, blood samples were withdrawn through the ocular vein. The circulation retention of activity was evaluated, assuming the total blood volume of the subject to be 7% of the total body weight.

Tissue-to-Organ Distribution Studies. To evaluate the distribution of [^{99m}Tc]Tc-DTPA-bis(ChoEA), healthy BALB/c mice, PC3, A549, and HCT116 tumor-xenografted mouse models were injected intravenously with 0.37 MBq of the radioconjugate in a 100 μL volume. The biodistribution studies of ^{18}F-FECH (10, 30, 60 min) were carried out in healthy BALB/c mice by administering 5 MBq of ^{18}F-FECH. The animals were sacrificed and dissected. The animals were sacrificed at 15 min, 45 min, 1, 2, and 4 h postinjection. The tumors, blood, liver, kidneys, and other major organs were collected, rinsed in PBS, and weighed. Decay-corrected uptake of the radiotracer in each organ was determined as the percentage injected dose per gram of tissue.

Small-Animal Imaging. Whole-body MicroSPECT imaging of [^{99m}Tc]Tc-DTPA-bis(ChoEA) was carried out in athymic mice with subcutaneous PC3, A549, and HCT116 tumors and healthy BALB/c mice. Each mouse was injected intravenously with 37 MBq of radiolabeled DTPA-bis(ChoEA) through the tail vein 1 h prior to imaging. MicroPET imaging was also carried out in healthy BALB/c mice with the administration of 10 MBq of [^{18}F]F-FECH, and reconstructed processed images were generated. All SPECT and PET images were reconstructed, and semiquantitative analysis was performed for the acquired images to assess tumor distribution and localization.

Dosimetry. The absorbed dose from [^{99m}Tc]Tc-DTPA-bis(ChoEA) was calculated using OLINDA software (version OLINDA/EXM 1.0, Vanderbilt University, USA). The software uses the medical internal radiation dose method for the calculation of doses from internally administered radiopharmaceuticals. The residence time in various source organs was calculated from the uptake studies and time−activity curves obtained for the control and athymic mice. The relative organ-mass scaling method was used to obtain the corresponding values of residence times in humans. This was used as an input in the software to obtain the absorbed dose estimates.

Data Analysis and Statistics. All data are presented as mean ± standard deviation. Data were analyzed using VIVID (AMIRA 4.1.1, San Diego, USA) GraphPad Prism 5.0 software. P values of less than 0.05 were considered statistically significant.

■ ASSOCIATED CONTENT

Supporting Information

The Supporting Information is available free of charge at https://pubs.acs.org/doi/10.1021/acsomega.1c04256.

All the characterization data of organic synthesis including NMR and mass spectra; HRMS results of the final compound and rhenium complex; in vitro toxicity studies; radiolabeling and serum stability; radiochromatogram showing the formation of a single species; serum stability of [^{99m}Tc]Tc-DTPA-bis-(ChoEA) in silico docking studies; tumor-to-muscle, tumor-to-blood, and tumor-to-liver values from PC3, A549, and HCT116 imaging studies calculated by the semiquantitative analysis of the MicroSPECT images; and the first in-human clinical trial data (PDF)

■ AUTHOR INFORMATION

Corresponding Authors

Puja Panwar Hazari − *Division of Cyclotron and Radiopharmaceutical Sciences, Institute of Nuclear Medicine and Allied Sciences, Delhi 110054, India;* orcid.org/0000-0003-4842-0728; Phone: +91-11-2390-5244; Email: puja.hazari@gmail.com, puja.inmas@gov.in; Fax: +91-11-2391-9509

Anil Kumar Mishra − *Division of Cyclotron and Radiopharmaceutical Sciences, Institute of Nuclear Medicine and Allied Sciences, Delhi 110054, India;* orcid.org/0000-0003-2523-9045; Phone: +91-11-2398-4480; Email: akmishra63@gmail.com; Fax: +91-11-2391-9509

Authors

Ambika Parmar Jaswal − *Division of Cyclotron and Radiopharmaceutical Sciences, Institute of Nuclear Medicine and Allied Sciences, Delhi 110054, India;* Present Address: Department of Neurological Surgery, UPMC Children's Hospital of Pittsburgh, USA

Surbhi Prakash − *Division of Cyclotron and Radiopharmaceutical Sciences, Institute of Nuclear Medicine and Allied Sciences, Delhi 110054, India*

Pallavi Sethi − *Division of Cyclotron and Radiopharmaceutical Sciences, Institute of Nuclear Medicine and Allied Sciences, Delhi 110054, India*

Aruna Kaushik − *Department of Nuclear Medicine, Institute of Nuclear Medicine and Allied Sciences, Delhi 110054, India*

Bal G. Roy − *Experimental Animal Facility, Institute of Nuclear Medicine and Allied Sciences, Delhi 110054, India*

Swati Kathait − *Division of Cyclotron and Radiopharmaceutical Sciences, Institute of Nuclear Medicine and Allied Sciences, Delhi 110054, India*

https://doi.org/10.1021/acsomega.1c04256
ACS Omega 2022, 7, 12509−12523

Baljinder Singh − *Post Graduate Institute of Medical Education & Research, Chandigarh 160012, India*

Complete contact information is available at: https://pubs.acs.org/10.1021/acsomega.1c04256

Author Contributions

Writing the original draft, investigation, and literature analysis: A.P.J. and P.P.H.; conceptualization, figures, project guidance, and supervision: P.P.H. and A.K.M. In vitro and animal experimentation: A.P.J., P.P.H., P.S., and B.G.R.; biodosimetry: A.K. and M.M.; studies: S.K. and P.P.H. Clinical SPECT scan: B.S. All authors have read and approved the final manuscript.

Notes

The authors declare no competing financial interest.

■ ACKNOWLEDGMENTS

The present work was supported by the Defence Research and Development Organization, Ministry of Defence, Delhi. The authors also acknowledge the grants received under the collaborative project of INMAS-SAMEER funded by the Ministry of Electronics and Information Technology (MeitY), India. The authors also extend their thanks to the Director, INMAS, for providing necessary facilities.

■ ABBREVIATIONS

CH, choline; FCH, fluorocholine; FECH, fluoroethyl choline; FDG, fluorodeoxyglucose; SPECT, single-photon emission tomography; CT, computed tomography; PET, positron emission tomography; 99mTc, technetium 99m; DTPA, diethylenetriaminepentaacetic acid; ROI, region of interest; %ID/g, percentage of injected dose per gram; ITLC, instant thin-layer chromatography; ChT, choline transporters

■ REFERENCES

(1) Hanahan, D.; Weinberg, R. A. Hallmarks of Cancer: the next Generation. *Cell* **2011**, *144*, 646−674.
(2) Bisdas, S.; Reimold, M.; Naegele, T.; Ernemann, U. Metabolic mapping of Gliomas Using Hybrid MR-PET Imaging: Feasibility of the method and spatial distribution of Metabolic Changes. *Invest. Radiol.* **2013**, *48*, 295−301.
(3) Abrantes, A. M.; Marques, I. A.; Botelho, M. F. Tumor functional Imaging by PET. *Biochim. Biophys. Acta (BBA)-Mol. Basis Dis.* **2020**, *1866*, 165717.
(4) Huang, J. Y.; Koh, W. P.; Yuan, J. M. A prospective evaluation of serum methionine-related metabolites in relation to pancreatic cancer risk in two prospective cohort studies. *Int. J. Cancer* **2020**, *147*, 1917−1927.
(5) Vander Heiden, M. G. Targeting cancer metabolism: a therapeutic window opens. *Nat. Rev. Drug Discov.* **2011**, *10*, 671−684.
(6) Wetter, A.; Lipponer, C.; Nensa, F.; Beiderwellen, K.; Olbricht, T.; Rübben, H.; Bockisch, A.; Schlosser, T.; Heusner, T. A.; Lauenstein, T. C. Simultaneous^{18}F Choline Positron Emission Tomography/ Magnetic resonance Imaging of the Prostate: Initial Results. *Invest. Radiol.* **2013**, *48*, 256−262.
(7) Mignion, L.; Gallez, B.; Jordan, B. F. Non-invasive in vivo imaging of early metabolic tumor response to therapies targeting choline metabolism. *Int. J. Cancer* **2016**, *138*, 2043−2049.
(8) Arlauckas, S. P.; Poptani, H.; Delikatny, E. J. Near infrared fluorescent imaging of choline kinase alpha expression and inhibition in breast tumors. *Oncotarget* **2017**, *8*, 16518−16530.
(9) Bagnoli, M.; Iorio, E.; Mezzanzanica, D. Choline Metabolism Alteration: A Focus on Ovarian Cancer. *Front. Oncol.* **2016**, *6*, 153.
(10) Esseridou, A.; Di Leo, G.; Sconfienza, L. M.; Caldiera, V.; Raspagliesi, F.; Grijuela, B.; Hanozet, F.; Podo, F.; Sardanelli, F. In vivo Detection of Choline in Ovarian Tuors using #D Magnetic Resonance Spectroscopy. *Invest. Radiol.* **2011**, *46*, 377−382.
(11) Juan, C. L.; Joaquín, M. C. Preclinical Characterization of RSM-932A, a Novel Anticancer Drug Targeting the Human Choline Kinase Alpha, an Enzyme Involved in Increased Lipid Metabolism of Cancer Cells. *Mol. Cancer Ther.* **2015**, *14*, 31−39.
(12) Trousil, S.; Lee, P.; Keun, H. C.; Sharma, R. Alterations of choline phospholipid metabolism in endometrial cancer are caused by choline kinase alpha overexpression and a hyperactivated deacylation pathway. *Cancer Res.* **2014**, *74*, 6867−6877.
(13) de Molina, A. R.; Sarmentero, E. J.; Belda, I. C.; Taron, M.; Cejas, M. V. P.; Skrzypski, M.; Ortega, G. D. Expression of choline kinase alpha to predict outcome in patients with early-stage non-small-cell lung cancer :a retrospective study. *Lancet Oncol.* **2007**, *8*, 889−897.
(14) Lacal, J. C. Choline kinase as a precision medicine target for therapy in cancer, autoimmune diseases and malaria. *Precis. Med.* **2015**, *2*, No. e980.
(15) Penet, M.-F.; Shah, T.; Maitra, A.; Bhujwalla, Z. M. Metabolic imaging of pancreatic ductal adenocarcinoma detects altered choline metabolism. *Clin. Cancer Res.* **2015**, *21*, 386−395.
(16) Leyton, J.; Smith, G.; Nguyen, Q.-D.; Robins, E.; Årstad, E.; Aboagye, E. O. [^{18}F]fluoromethyl-[1,2-$^{2}H_4$]-choline: a novel radiotracer for imaging choline metabolism in tumors by positron emission tomography. *Cancer Res.* **2009**, *69*, 7721−7728.
(17) Heijmink, S. W. T. P. J.; van Lin, E. N. J. T.; Heerschap, A.; Barenstz, J. O. Prostate and Lymph Node Proton Magnetic Resonance (MR) Spectroscopic Imaging with external Array coils to detect Recurrent Prostate Cancer after Radiation Therapy. *Invest. Radiol.* **2007**, *42*, 420−427.
(18) Michel, V.; Yuan, Z.; Barenstz, J. O. Choline transport for phospholipid synthesis. *Exp. Biol. Med.* **2006**, *231*, 490−504.
(19) Yoshimoto, M.; Waki, A.; Yonekura, Y.; Fujibayashi, Y. Radiolabeled choline as a proliferation marker: Comparison with radiolabeled acetate. *Nucl. Med. Biol.* **2004**, *31*, 859−865.
(20) Hara, T.; Bansal, A.; DeGrado, T. R. Choline transporter as a novel target for molecular imaging of cancer. *Mol. Imag.* **2006**, *5*, 7290.2006.00032.
(21) Filippi, L.; Orazio, S.; Oreste, B. Recent advances in PET probes for hepatocellular carcinoma characterization. *Expet Rev. Med. Dev.* **2019**, *16*, 341−350.
(22) Witney, T. H.; Alam, I. S.; Awais, R. O.; Aboagye, E. O. Evaluation of Deuterated ^{18}F- and ^{11}C-labeled Choline Analogs for Cancer detection by Positron Emission Tomography. *Clin. Cancer Res.* **2012**, *18*, 1063−1072.
(23) DeGrado, T. R.; Polascik, T. J.; Price, D. T. Synthesis and evaluation of ^{18}F-labeled choline as an oncologic tracer for positron emission tomography: initial findings in prostate cancer. *Cancer Res.* **2001**, *61*, 110−117.
(24) Devés, R.; Krupka, R. M. The binding and translocation steps in transport as related to substrate structure: a study of the choline carrier of erythrocytes. *Biochim. Biophys. Acta* **1979**, *557*, 469−485.
(25) Clary, G. L.; Tsai, C.-F.; Guynn, R. W. Substrate specificity of choline kinase. *Arch. Biochem. Biophys.* **1987**, *254*, 214−221.
(26) Hara, T.; Kosaka, N.; Hiroichi, H. Development of 18F-fluoroethylcholine for cancer imaging with PET: synthesis, biochemistry, and prostate cancer imaging. *J. Nucl. Med.* **2002**, *43*, 187−199.
(27) Chen, W.; Schiepers, C.; Cloughesy, T. ^{18}F-FDOPA PET imaging of brain tumors: comparison study with ^{18}F-FDGPETand evaluation of diagnostic accuracy. *J. Nucl. Med.* **2006**, *47*, 904−911.
(28) Onyeuku, N. E.; Ayala-Peacock, D. N.; Garg, P.; Blackstock, W. ^{11}C-Choline PET-CT Detection of Osseous Metastases versus Bone Scan in Newly Diagnosed High Risk Prostate Cancer Patients-A Pilot Study. *J. Nucl. Med. Radiat. Ther. S* **2013**, *6*, 2.
(29) Sanders, V. A.; Iskhakov, D.; Abdel, D. A. Synthesis, characterization and biological studies of rhenium, technetium-99m and rhenium-188 pentapeptides. *Nucl. Med. Biol.* **2019**, *68*, 1−13.

(30) Workman, P.; Aboagye, E. O.; Aboagye, E. O.; Balkwill, F.; Balmain, A.; Bruder, G.; Chaplin, D. J.; Double, J. A.; Everitt, J.; Farningham, D. A. H.; Glennie, M. J.; et al. Guidelines for the welfare and use of animals in cancer research. *Br. J. Cancer* **2010**, *102*, 1555−1577.
(31) Papagiannopoulou, D. Technetium-99m radiochemistry for pharmaceutical applications. *J. Labelled Compd. Radiopharm.* **2017**, *60*, 502−520.
(32) Malito, E.; Sekulic, N.; Too, W. C. S.; Konrad, M.; Lavie, A. Elucidation of Human Choline Kinase Crystal Structure in complex with the products ADP and Phosphocholine. *J. Mol. Biol.* **2006**, *364*, 136−151.
(33) Morris, G. M.; Huey, R.; Lindstrom, W.; Olson, A. J. AutoDock4 and AutoDockTools4: Automated Docking with selective receptor flexibility. *J. Comput. Chem.* **2009**, *30*, 2785−2791.
(34) Glunde, K.; Bhujwalla, Z. M. Metabolic Tumor Imaging using Magnetic resonance Spectroscopy. *Semin. Oncol.* **2011**, *38*, 26−41.
(35) Sharma, R.; Aboagye, E. Development of radiotracers for oncology-the interface with pharmacology. *Br. J. Pharmacol.* **2011**, *163*, 1565−1585.
(36) Hara, T.; Kosaka, N.; Kishi, H. PET imaging of prostate cancer using carbon-11-choline. *J. Nucl. Med.* **1998**, *39*, 990−995.
(37) Hara, T.; Kosaka, N.; Shinoura, N.; Kondo, T. PET imaging of brain tumor with [methyl-[^{11}C]choline. *J. Nucl. Med.* **1997**, *38*, 842−847.
(38) Kotzerke, J.; Gschwend, J. E.; Neumaier, B. PET for prostate cancer imaging: still a quandary or the ultimate solution? *J. Nucl. Med.* **2002**, *43*, 200−202.
(39) Cimitan, M.; Bortolus, R.; Morassut, S.; Trovò, M. G. [^{18}F]-fluorocholine PET/CT imaging for the detection of recurrent prostate cancer at PSA relapse: experience in 100 consecutive patients. *Eur. J. Nucl. Med.* **2006**, *33*, 1387−1398.
(40) Arano, Y. Recent advances in 99mTc Radiopharmaceuticals. *Ann. Nucl. Med.* **2002**, *16*, 79−93.
(41) Singh, N.; Hazari, P. P.; Prakash, S.; Mishra, A. K. A homodimeric bivalent radioligand derived from 1-(2-methoxyphenyl)piperazine with high affinity for in-vivo 5HT1A receptor imaging. *MedChemComm* **2012**, *3*, 814−823.
(42) Numata, J.; Juneja, A.; Diestler, D. J.; Knapp, E.-W. Influence of Spacer-Receptor Interactions on the stability of Bivalent Ligand−Receptor Complexes. *J. Phys. Chem. B* **2012**, *116*, 2595−2604.
(43) Schepkens, C.; Dallons, M.; Dehairs, J. A New Classification Method of Metastatic Cancers Using a ^{1}H-NMR-Based Approach: A Study Case of Melanoma, Breast, and Prostate Cancer Cell Lines. *Metabolites* **2019**, *9*, 281.
(44) Shingo, B.; James, E.; Richard, W. Choline uptake and RNA expression profile in cancerous and normal prostate cell lines: No significant role of choline transporter in PET tracer uptake. *J. Nucl. Med.* **2007**, *48*, 335.
(45) Ling, C. S.; Yin, K. B.; Cun, S. T. W.; Ling, F. L. Expression profiling of choline and ethanolamine kinases in MCF7, HCT116 and HepG2 cells, and the transcriptional regulation by epigenetic modification. *Mol. Med. Rep.* **2015**, *11*, 611−618.
(46) Stabin, M.; Taylor, A. J.; Eshima, D.; Wooter, W. Radiation dosimetry for technitium-99m-MAG3, technitium -99m-DTPA, and iodine-131-OIH based on human biodistribution studies. *J. Nucl. Med.* **1992**, *33*, 33−40.
(47) Sawicki, L. M.; Schaarschmidt, B. M.; et al. Prospective Comparison of whole −body MRI and 68ga-PSMA PET/CT for the detection of biochemical recurrence of prostate cancer after radical prostatectomy. *Eur. J. Nucl. Med. Mol. Imag.* **2019**, *46*, 1542−1550.
(48) Afshar-Oromieh, A.; Eisenhut, M.; Holland-Letz, T.; et al. Comparison of PET imaging with a 68Ga−labelled PSMA ligand and 18F- Choline −based PET/CT for the diagnosis of recurrent Prostate cancer. *Eur. J. Nucl. Med. Mol. Imag.* **2014**, *41*, 11−20.
(49) Schwenck, J.; Kruck, S.; Stenzl, A.; Nikolaou, K.; Pfannenberg, C.; la Fougère, C. Comparison of ^{68}Ga-labelled PSMA-11 and 11C-choline in the detection of prostate cancer metastases by PET/CT. *Eur. J. Nucl. Med. Mol. Imag.* **2017**, *44*, 92−101.
(50) Giovacchini, G.; Ciarmiello, A.; Picchio, M. ^{11}C-choline PET/CT predicts survival in prostate cancer patients with PSA < 1 ng/ml. *Eur. J. Nucl. Med. Mol. Imag.* **2019**, *46*, 921−929.
(51) O'Boyle, N. M.; Banck, M.; James, C. A.; et al. Open Babel: An open chemical toolbox. *J. Cheminf.* **2011**, *3*, 33.
(52) Trott, O.; Arthur, J. AutoDock Vina: Improving the Speed and Accuracy of docking with new scoring function, efficient optimization, and multithreading. *J. Comput. Chem.* **2010**, *31*, 455−461.
(53) *Discovery Studio Visualizer Software*. Version 4.0, 2020. Retrieved from http://www.accelrys.com.

https://doi.org/10.1021/acsomega.1c04256
ACS Omega 2022, 7, 12509−12523